Supplementary Information

Tailoring Alkyl Chain Length of linear ester in Moderately Concentrated Electrolyte for High-Performance Graphite Anode in K-Ion Batteries

Experiment Section

Materials and Chemicals: Potassium Chunk was purchased from Aladdin Reagent Co., Ltd., Potassium bis(fluoroslufonyl)imide (KFSI) salt was purchased from TCI Reagent Co., Ltd. EC, DMC, EMC, and DEC were purchased from Sigma-Aldrich. MPC and BMC were provided by BTR New Material Group Co., Ltd. All the salts and solvents were commercial battery-grade products and used as received without further purification.

Preparation of Electrolytes: The moderately concentrated ester-based electrolytes were prepared by dissolving 2.4 M KFSI into mixtures of EC and linear ester (DMC, EMC, DEC, MPC, BMC) (v:v = 3:7), and then stirred overnight in an argon-filled glovebox (<1.0 ppm O_2 and <0.1 ppm H_2O). When preparing dilute, moderately concentrated, and highly concentrated ester-based electrolytes, 0.8 M, 2.4 M or 4.0 M KFSI salts was used, and the solutions were then stirred overnight in argon-filled glovebox.

Preparation of Graphite and PTCDA Electrodes: A slurry composed of 80 wt% natural graphite powder (Sigma-Aldrich), 10 wt% carbon black, and 10 wt% polyacrylic acids (PAA, Sigma-Aldrich) binder with deionized water was uniformly cast onto Cu foils (16 mm in diameter) and then dried at 100 ℃ for 12 h to obtain the graphite electrode. Commercial 3,4,9,10-perylene-tetracarboxylic acid-dianhydride (denoted as PTCDA) was purchased from Sigma Aldrich. Before to use in the cathode of full-cells, the PTCDA was annealed at 450 ℃ for 4 h under Ar atmosphere with a heating rate of 5 ℃ min^{-1}. The PTCDA cathode was prepared by mixing annealed PTCDA, carbon black, and PAA binder in a weight ratio of 8:1:1 to form a slurry, and casting onto the Al foil, followed by drying at 80 ℃ for 12 h. The average mass loading of the graphite and PTCDA electrode was about 1.6 and 2.0 mg cm^{-2}, respectively.

Electrochemical Measurements: All the electrochemical tests were performed in the 2032-type coin cells. The K/graphite (K/Gr) half-cells were assembled with the graphite electrode, hand-made potassium foil as the anode, and a glass-fiber separator (Whatman, Grade GF/B). 80 μL electrolyte was added to each cell. For the Gr/PTCDA full-cells, the graphite electrode was pre-potassiated in a K/Gr half-cell as the anode, while the PTCDA cathode was also pre-cycled for 3 times. To avoid K plating on graphite, the cathode/anode capacity ratio was chosen to 0.96:1. The galvanostatic measurements were carried out on a LAND CT2001A battery-testing system in the potential range of 0.01 to 2.5 V (vs. K^+/K) for the K/Gr half-cell, and 1.0 to 3.0 V (vs. K^+/K) for the Gr/PTCDA full-cell. Ionic conductivities of electrolytes were measured in a homemade vial with two glassy carbon electrodes separated by 0.5 cm in a Teflon holder. Before the conductivity tests, the calibration was performed using a standard 0.01 M KCl aqueous solution at 25 ℃. The electrochemical impedance spectra of graphite/graphite symmetric cells were recorded on an electrochemical workstation (Biologic, VSP-300) in the frequency range between 100 kHz and 0.01 Hz with AC voltage amplitude of 10 mV. Two graphite electrodes are potassiated up to the half theoretical capacity (0.5 moles of K per 8 moles of C) under 0.1 C. By this approach, the graphite/electrolyte interfaces are identical for both electrodes and the SEI is identical in composition and thickness.

Material Characterizations: The viscosity of electrolytes was measured with an Anton-Paar SVM3001 viscometer. While the density of the electrolytes was determined by measuring the weight of 1.0 mL prepared solutions. During the testing processes of the viscosity and density, all the samples were kept at 25 ℃. Raman spectroscopy (Thermo Fisher, DXR2) was used to analyze the coordination structures of various electrolytes. A solid-state laser with a wavelength of 532 nm was adopted. Transmission electron microscopy (TEM, Titan G260-300, 200 kV) and X-ray photoelectron spectroscopy (XPS, Thermo escalab 250Xi) were employed to analyze the thickness, chemical composition of the SEI films, respectively. The cycled coin cells were disassembled in the glovebox, and the cycled graphite electrodes were rinsed by corresponding linear ester solvents several times to remove the residual potassium salts. Then the obtained

electrodes were dried in an argon-filled glovebox and characterized by XPS under the Ar protection. The etching depth of Ar^+ ion sputtering for the depth profiling XPS was 2 nm. XPS curves were fitted by the CasaXPS program with Gaussian–Lorentzian function after subtraction of a Shirley background. The fitting errors of XPS test results using this method are within ±1 %.

Computational Details: The solvation energies and desolvation energies of K^+-solvent complexes were calculated using the Gaussian g09 package.[1] Among the several density functional theory methods, the Perdew–Burke–Ernzerhof (PBE) functionals with 6-31+G(d,p) basis set were selected to optimize all the geometries of K^+-solvent complexes based on the previous work.[2] First, the thermodynamic stability of K^+-solvent complexes was evaluated by calculating the solvation energy (E_s) values in different electrolytes. E_s of K^+-ester complex can be defined as:

$$E_s = E_{[K^+ - (EC)_m(linear\ ester)_n]} - m \times E_{EC} - n \times E_{linear\ ester} - E_{K^+} \quad (m+n=5) \tag{1}$$

where $E_{[K^+ - (EC)_m(linear\ ester)_n]}$ is the energy of the K^+-ester complex, $E_{EC}$and $E_{linear\ ester}$ are the energy of the solvent molecule, and E_{K^+} is the energy of K^+. Then, the desolvation energy (E_{des}) values of the K^+-$(EC)_m$(linear ester)$_n$ ($n \geq 1$) complexes were calculated using the follow equations:

$$E_{des} = E_{[K^+ - (EC)_m(linear\ ester)_{n-1}]} + E_{linear\ ester} - E_{[K^+ - (EC)_m(linear\ ester)_n]} \tag{4}$$

[1] F. Ogliaro, M. Bearpark, J. Heyd, E. Brothers, K. Kudin, V. Staroverov, R. Kobayashi, J. Normand, K. Raghavachari, A. Rendell, Gaussian 09, revision a. 02. gaussian, Inc.: Wallingford, CT, (2009).

[2] O. Borodin, M. Olguin, P. Ganesh, P. R. C. Kent, J. L. Allen, W. A. Henderson, Phys. Chem. Chem. Phys. 2016, 18, 164.

Table S1 Viscosity and ionic conductivity of electrolytes

Electrolyte	Viscosity (mPa S^{-1})	Conductivity (mS cm^{-1})
0.8 M EC+DMC	2.73	14.72
4.0 M EC+DMC	18.14	4.01
2.4 M EC+DMC	8.22	10.08
2.4 M EC+EMC	8.51	9.79
2.4 M EC+MPC	9.12	8.31
2.4 M EC+DEC	9.16	7.05
2.4 M EC+BMC	9.45	6.44

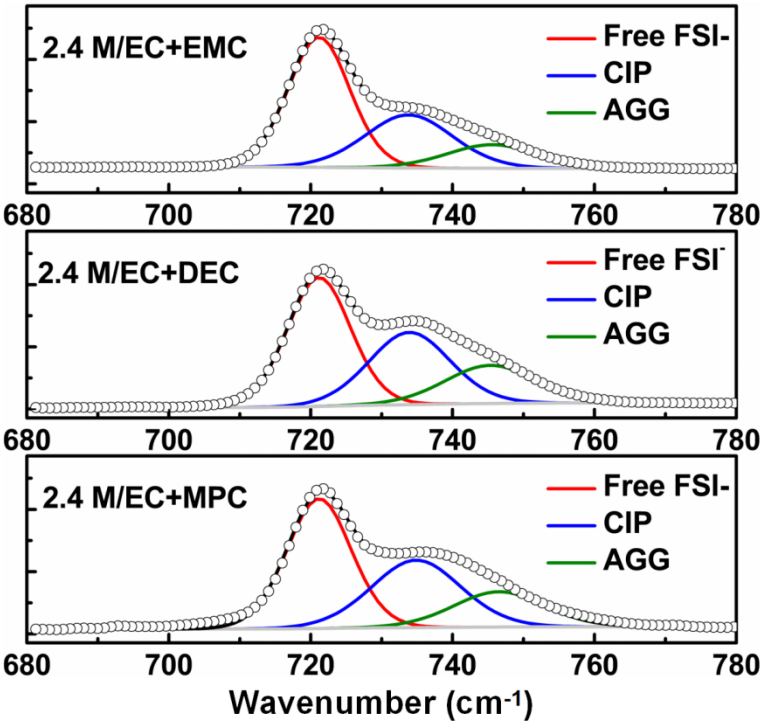

Fig. S1 Raman spectra of 2.4 M KFSI/EC+EMC, 2.4 M KFSI/EC+DEC, and 2.4 M KFSI/EC+MPC electrolytes in the wavenumber range of 680-780 cm^{-1}.

Table S2 Distributions of FSI-based clusters in the MC electrolytes

Electrolyte	Free FSI^- (%)	CIP (%)	AGG (%)
0.8 M EC+DMC	88.8	11.2	0
4.0 M EC+DMC	0	45.2	54.8
2.4 M EC+DMC	57.2	30.1	12.7
2.4 M EC+EMC	54.1	31.4	14.5
2.4 M EC+MPC	47.6	34.2	18.2
2.4 M EC+DEC	46.9	33.8	19.3
2.4 M EC+BMC	45.2	30.3	24.5

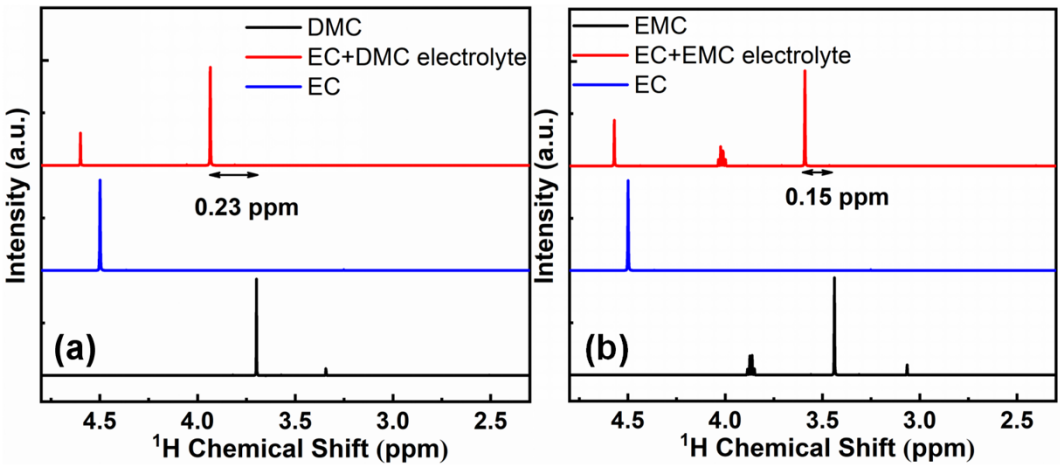

Fig. S2 ^{1}H NMR spectra of (a) 2.4 M KFSI/EC+DMC and (b) 2.4 M KFSI/EC+EMC electrolytes.

A smaller ^{1}H down-field shift (0.15 ppm) for the nearby methyl (δ = 3.5~4.0 ppm) can be investigated in the NMR spectra of 2.4 M KFSI/EC+EMC as compared to 2.4 M KFSI/EC+DMC (0.23 ppm). The down-field shift of the ^{1}H NMR signals indicates a shift of electron clouds from H to C. When the interactions between the K^{+} and alkyl chain esters become weaker, fewer electrons are attracted from the oxygen on EMC molecules to K^{+}. There is a competition between the FSI^{-} anions and alkyl chain esters in the first K^{+} solvation shell. If the interactions between the K^{+} and alkyl chain esters have been strengthened, the K^{+}-FSI^{-} interaction will be weakened.

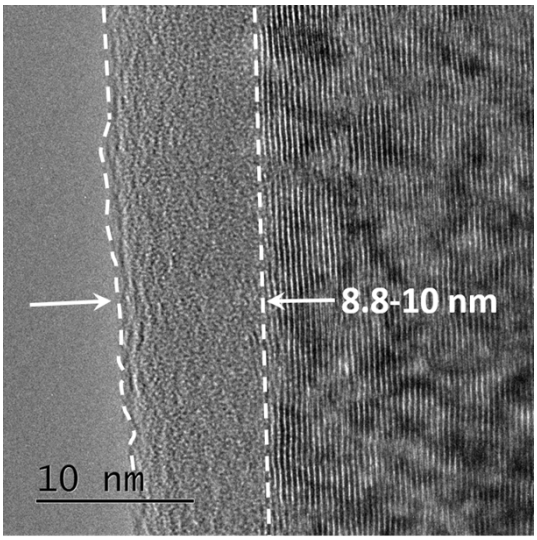

Fig. S3 High-resolution TEM images of graphite anodes cycled in 0.8 M KFSI/EC+DMC.

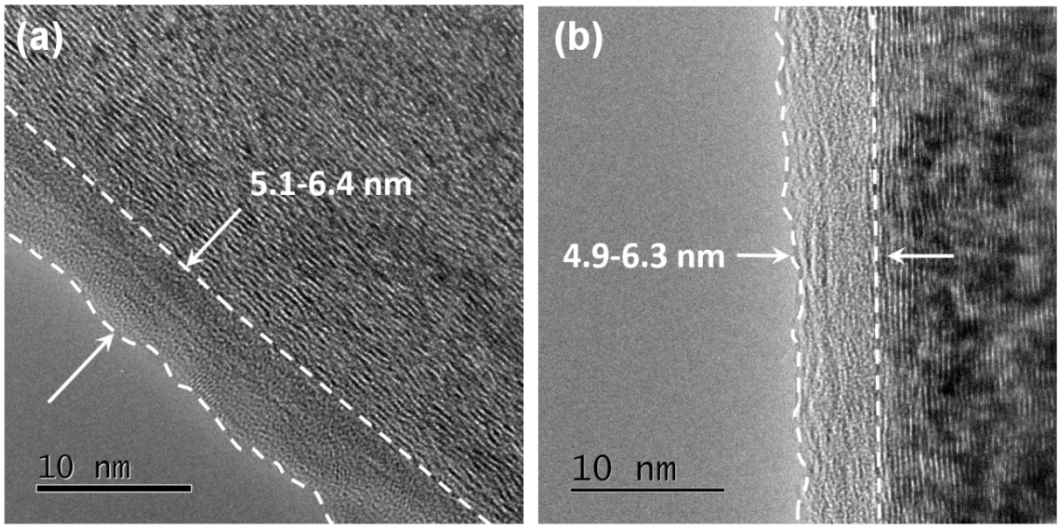

Fig. S4 High-resolution TEM images of graphite anodes cycled for 50 times in (a) 2.4 M KFSI/EC+DMC and (b) 2.4 M KFSI/EC+BMC.

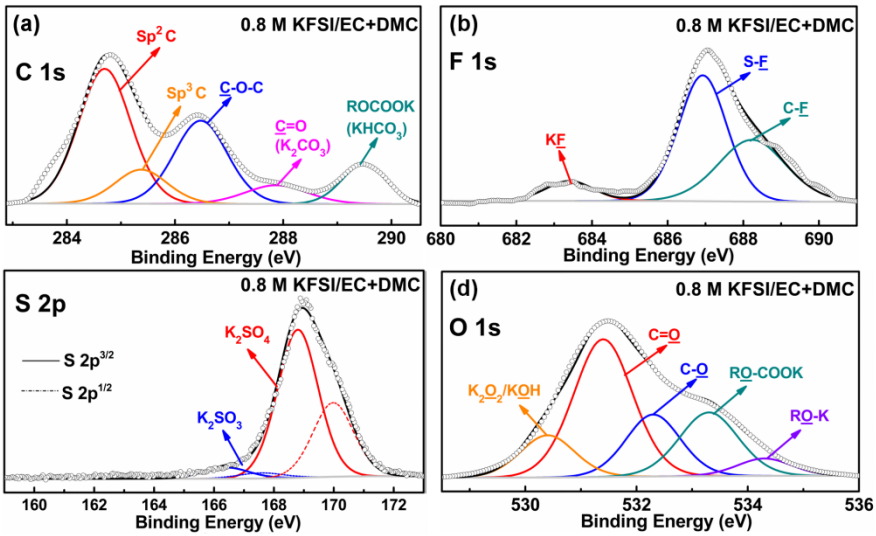

Fig. S5 High-resolution (a) C 1s, (b) F 1s, (c) S 2p, and (d) O 1s XPS spectra of graphite anodes cycled in 0.8 M KFSI/EC+DMC.

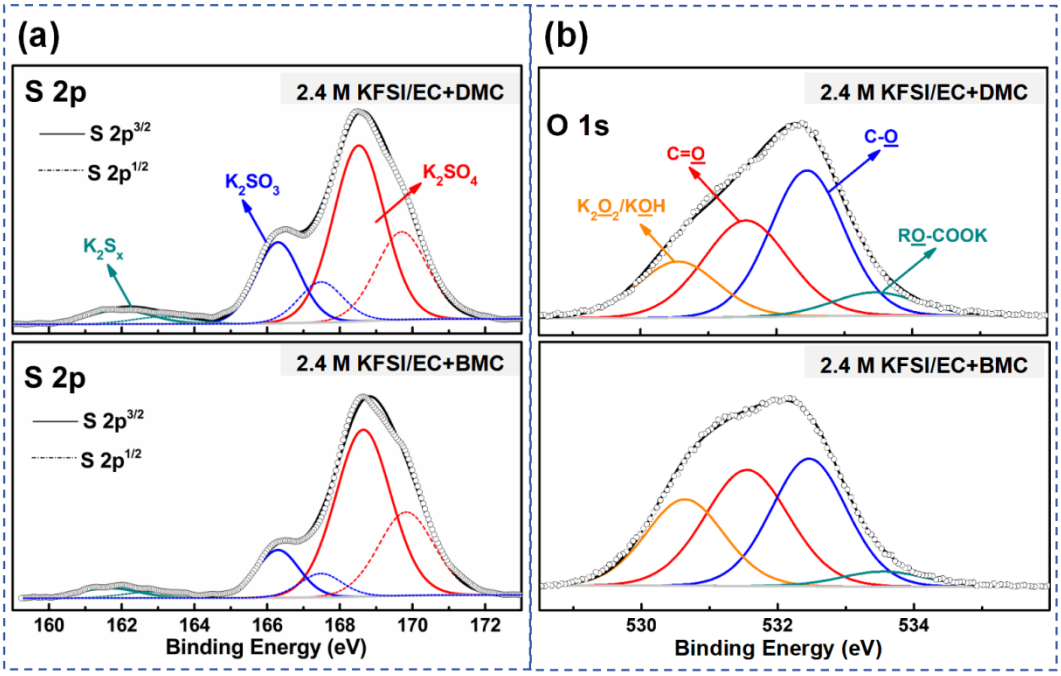

Fig. S6 High-resolution (a) S 2p, and (b) O 1s XPS spectra of graphite anodes cycled in 2.4 M KFSI/EC+DMC and 2.4 M KFSI/EC+BMC electrolytes.

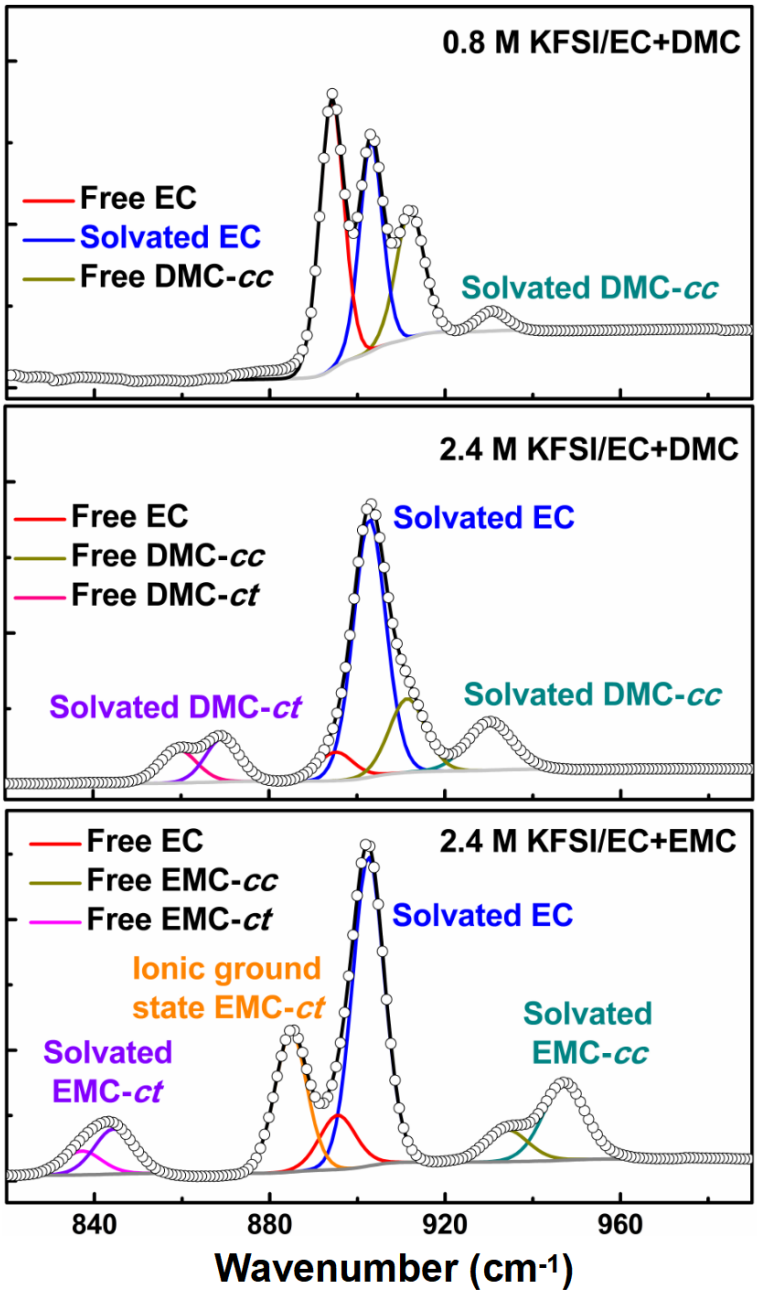

Fig. S7 Raman spectra of 0.8 M KFSI/EC+DMC, 2.4 M KFSI/EC+DMC, and 2.4 M KFSI/EC+EMC electrolytes in the wavenumber range of 820-990 cm^{-1}.

Raman peak assignments:

Free EC: 894 cm^{-1}, Solvated EC: 903 cm^{-1};

Free DMC-*cc*: 910 cm^{-1}, Solvated DMC-*cc*: 930 cm^{-1}, Free DMC-*ct*: 860 cm^{-1}, Solvated DMC-*ct*: 870 cm^{-1};

Free EMC-*cc*: 934 cm^{-1}, Solvated EMC-*cc*: 947 cm^{-1}, Free EMC-*ct*: 837 cm^{-1}, Solvated EMC-*ct*: 845 cm^{-1}, O-CH_2 stretching + CH_3-O-C stretching + CH_3-O-C bending of EMC-*ct*: 885 cm^{-1};

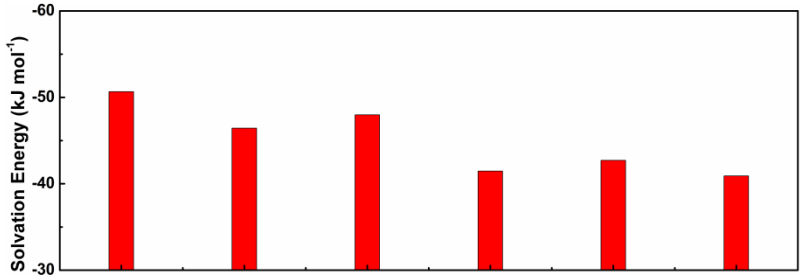

Fig. S8 E_s values of simulated K^+-$(EC)_m$(linear ester)$_n$ (m + n = 5) complexes.

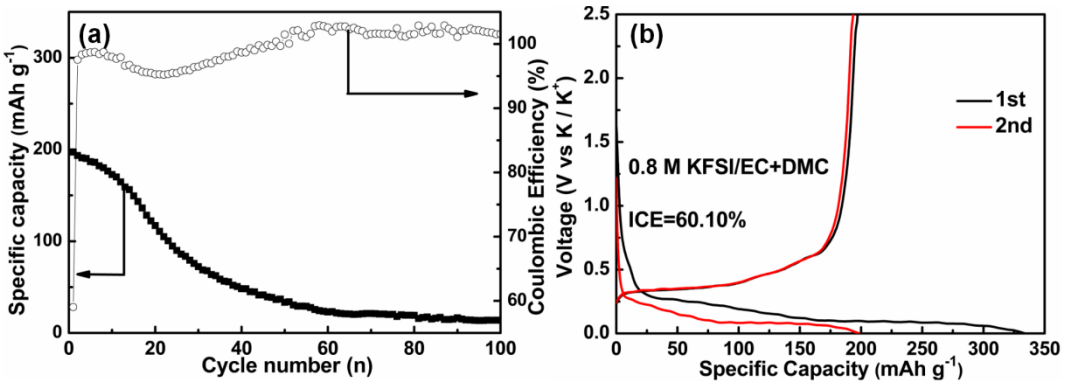

Fig. S9 (a) Cycling performance and (b) galvanostatic voltage profiles of graphite anode in 0.8 M KFSI/EC+DMC electrolyte at 0.5 C.

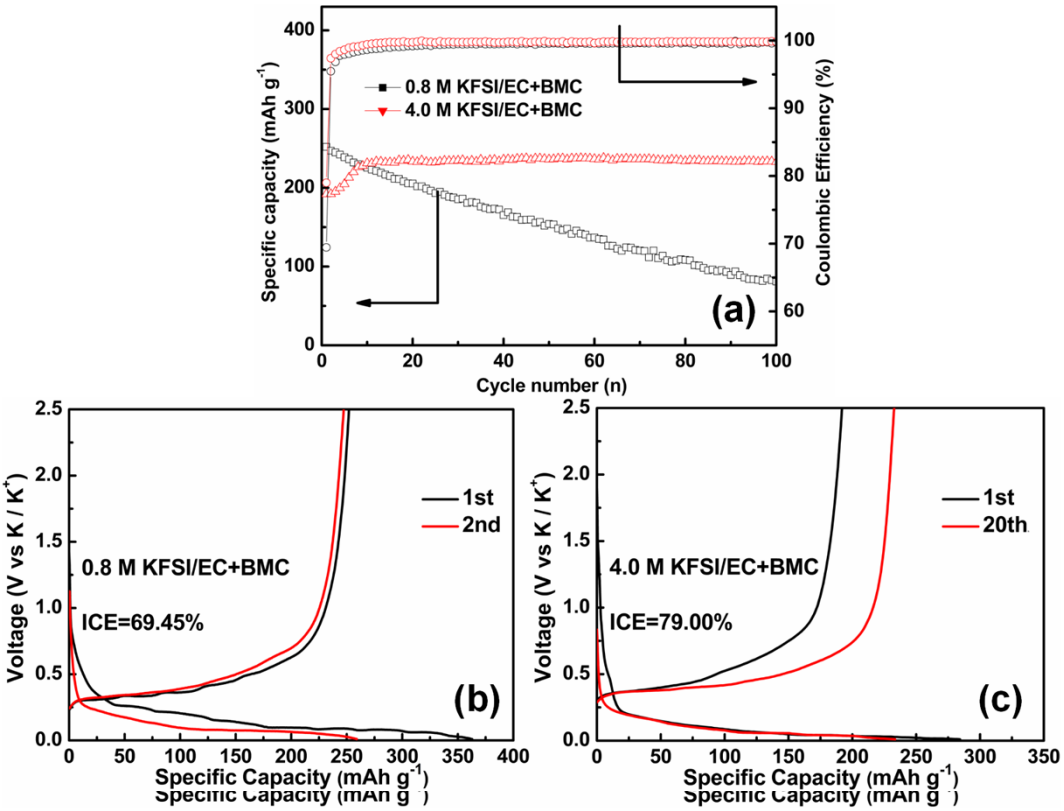

Fig. S10 (a) Cycling performance and voltage profiles of graphite anode in (b) 0.8 M KFSI/EC+BMC and (c) 4.0 M KFSI/EC+BMC electrolytes at 0.5 C.

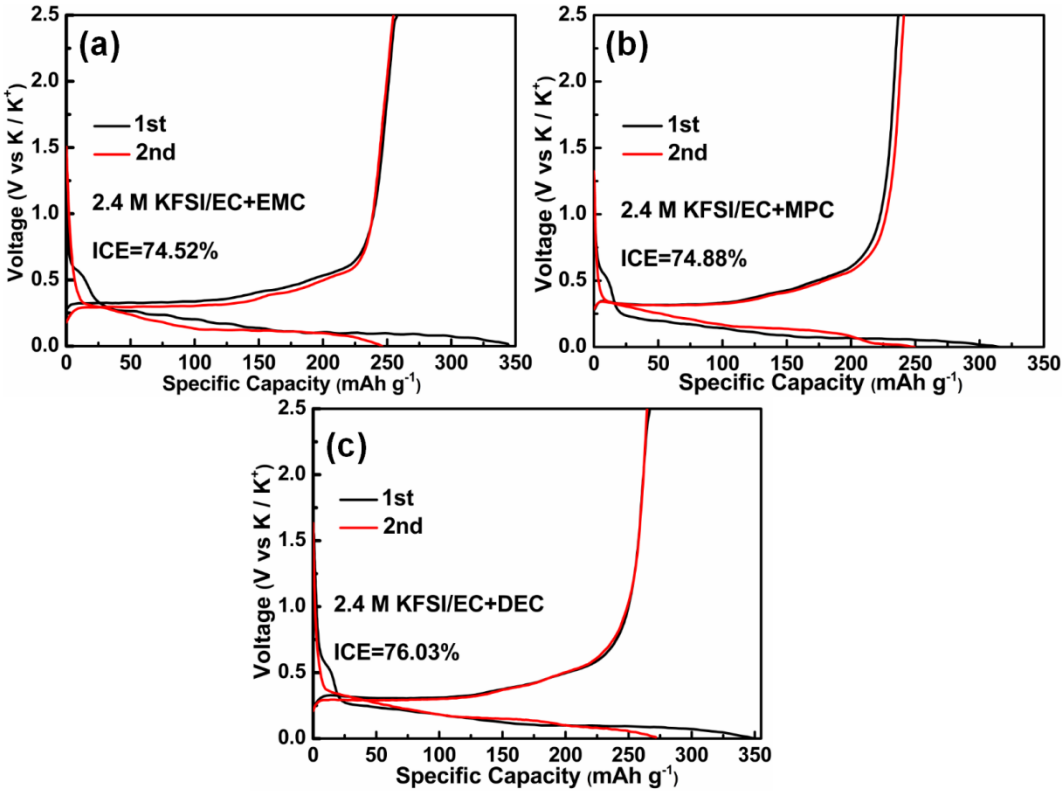

Fig. S11 Galvanostatic charge-discharge curves of graphite anode in (a) 2.4 M KFSI/EC+EMC, (b) 2.4 M KFSI/EC+MPC, and (c) 2.4 M KFSI/EC+DEC at 0.5 C.

Table S3 Performance of K/Gr half-cells using the MC electrolytes

Electrolyte	Initial Capacity (mAh g^{-1})	Initial Coulombic Efficiency (%)	Average Capacity within 100 cycles (mAh g^{-1})
2.4 M EC+DMC	169.3	70.06	215.1
2.4 M EC+EMC	246.8	74.52	234.0
2.4 M EC+MPC	236.8	74.88	250.3
2.4 M EC+DEC	267.3	76.03	256.9
2.4 M EC+BMC	273.3	77.94	269.3

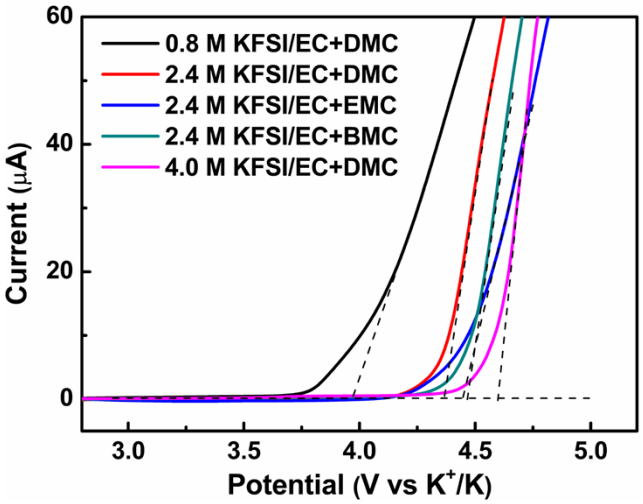

Fig. S12 LSV curves of K/Al cells with various electrolytes at 1 mV s^{-1}.

The 0.8 M KFSI/EC+DMC electrolyte has an oxidation onset potential of 3.9 V vs K^+/K due to the passivation of Al metal by the FSI^- anion. In contrast, this value is shifted to 4.35-4.45 V vs K^+/K in the cells using moderately concentrated (MC) electrolytes. Highly concentrated KFSI electrolyte revealed much enhanced oxidation durability and no significant anodic current was induced up to 4.6 V vs K^+/K.

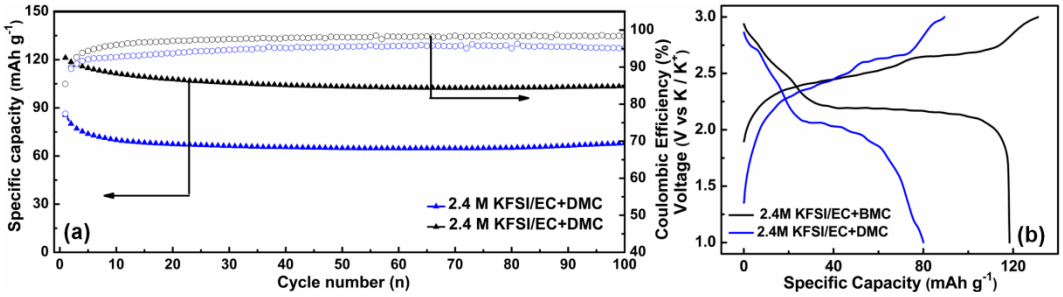

Fig. S13 (a) Cycling performance and (b) charge-discharge profiles (2nd cycle) of KIB full cells with 2.4 M KFSI/EC+DMC or 2.4 M KFSI/EC+BMC electrolyte at 200 mA g^{-1}. KIB full cells are based on the potassiated graphite anode and the annealed PTCDA cathode.

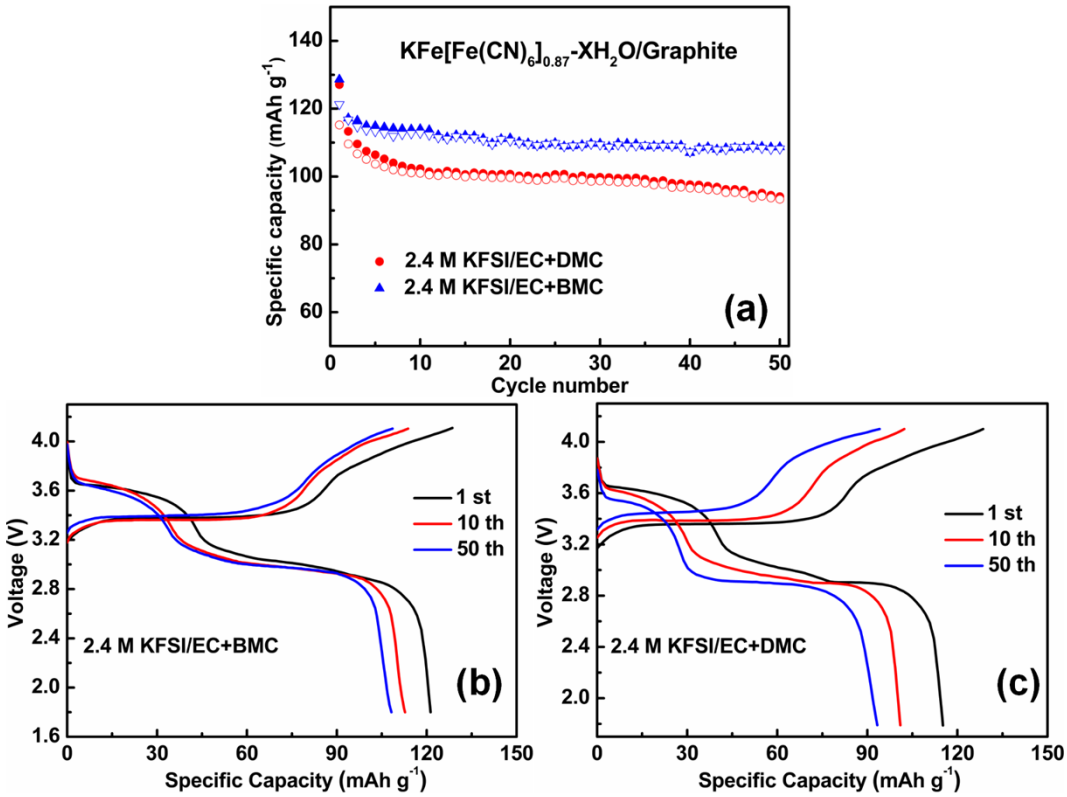

Fig. S14 (a) Cycling performance and voltage profiles of graphite/Prussian blue KIB full-cells with (b) 2.4 M KFSI/EC+BMC and (c) 2.4 M KFSI/EC+DMC electrolytes at 25 mA g^{-1}.

The hydrated hexacyanoferrate ($K_{1.48}Fe[Fe(CN)_6]_{0.87}\square_{0.13}\cdot 1.89H_2O$) PB framework was prepared via a simple precipitation route (*ACS Energy Lett. 2017, 2, 1122-1127*). Then, the graphite/PB KIB full-cells were assembled using a N/P ratio of 1:1.2, and their working voltage range is 1.8-4.1 V. The battery with 4.0 M KFSI/EC+BMC electrolyte shows an initial discharge capacity of 121.3 mAh g^{-1} at 25 mA g^{-1}, and its capacity retention is 89.2% after 50 cycles. In contrast, the battery with 4.0 M KFSI/EC+DMC electrolyte has a similar initial discharge capacity of 115.2 mAh g^{-1}, but only 81.0% capacity is retained after 50 cycles. In addition, the voltage gap between the charge and discharge profiles for the cell with 4.0 M KFSI/EC+DMC electrolyte is larger than that with 4.0 M KFSI/EC+BMC electrolyte.